Unexpected entanglement dynamics in semidilute blends of supercoiled and ring DNA

Karthik R. Peddireddy[1], Megan Lee[1], Yuecheng Zhou[2], Serenity Adalbert[1], Sylas Anderson[1], Charles M. Schroeder[2], Rae M. Robertson-Anderson[1,*]

[1]*Department of Physics and Biophysics, University of San Diego, 5998 Alcala Park, San Diego, CA 92110, United States*

[2]*Department of Materials Science and Engineering, Beckman Institute for Advanced Science and Technology & Department of Chemical and Biomolecular Engineering, University of Illinois at Urbana-Champaign, Urbana, IL 61801, United States*

Supporting Information

Expanded Experimental Section

DNA Preparation: Circular 50 kbp DNA molecules were prepared by replication of fosmid constructs in Escherichia coli, followed by extraction, purification and enzymatic treatment using protocols detailed elsewhere[1, 2] and briefly described below.

To replicate DNA, E. coli cultures containing the fosmid clone were grown from frozen glycerol stocks. To extract the DNA, cells were lysed via treatment with an alkaline solution. The extracted DNA was then renatured via treatment with an acidic detergent, precipitated in isopropanol, washed with 70% ethanol, and resuspended in TE buffer (10 mM Tris-HCl (pH 8), 1 mM EDTA).

To purify the DNA, the solution was treated with Rnase A (to remove contaminating RNA) followed by phenol-chloroform extraction and dialysis (to remove proteins). The final DNA solution, ~300 μL in volume, was stored in TE10 buffer (10 mM Tris-HCl (pH 8), 1 mM EDTA, and 10 mM NaCl) at 4°C. This buffer provides the DNA with good solvent conditions with a measured Flory exponent of ~0.59.[3]

We note that the ~300 μL volume is more than enough for many microrheology measurements (described below) that require ~10 μL per experiment; but it is prohibitively small for standard rheology measurements that require ~100 μL per experiment.

DNA Blend Characterization: The resulting 50 kbp DNA solution was analyzed via agarose gel electrophoresis to determine solution concentration and estimate the percentage of different DNA topologies comprising the sample. Gel analysis was performed using a Life Technologies E-Gel Imager and Gel Quant Express software. From the gel analysis, we determined that the purified solution had a total DNA concentration of 0.56 mg/mL and consisted of ~75% relaxed circular (*R*) molecules and ~25% supercoiled (*S*). We note that gel electrophoresis cannot accurately detect small (<5%) fractions of molecules in a sample, and loading the sample into the microscope chamber for experiments can introduce shear-induced nicks and cuts in the DNA that may not be present in the gel results.

To improve the accuracy of our blend composition determination, and determine the structure and heterogeneity of supercoiled constructs, we performed single-molecule 'counting' experiments described below. In these experiments, we directly imaged 231 randomly chosen molecules in the sample under flow to determine the topology of each molecule and establish sufficient statistics to determine the overall fraction of ring, supercoiled, and linear molecules in the sample. This method also allowed us to determine the structure that supercoiled constructs assumed (i.e. linear, branched, etc).

For counting experiments, 5 μL of the DNA blend was diluted 50x and fluorescently labeled with YOYO-1 (ThermoFisher) at a dye-to-base pair ratio of 1:4. A trace amount of labeled molecules was added to a viscous imaging buffer solution containing 10 mM Tris-HCl (pH 8), 1 mM EDTA, 10 mM NaCl and 60%

w/w sucrose. In addition, a small amount of reducing agent β-mercaptoethanol (14 μM) and coupled enzymatic oxygen scavenging system containing glucose (50 μg/mL), glucose oxidase (0.01 μg/mL), and catalase (0.004 μg/mL) were added to suppress photobleaching and photocleaving. The sample was then rotationally mixed for >20 minutes before introducing into the microfluidic cross-slot device, fabricated using standard techniques in soft lithography as described before.[4] In brief, the microfluidic device contained a fluidic layer situated below a control layer containing a fluidic valve. The fluidic layer was fabricated to contain a cross-slot channel geometry to generate planar extensional flow. All DNA molecules were then stretched under the same flow strength. Single-molecule imaging was performed using an inverted epifluorescence microscope (IX71, Olympus) and EMCCD camera (iXon, Andor Technology). Labeled DNA solutions were illuminated using a 50 mW 488 nm laser (Spectra-Physics, CA, USA) directed through a 2.2 neutral density filter (ThorLabs, NJ, USA) and a 488 nm single-edge dichroic (ZT488rdc, Chroma). Fluorescence emission was collected by a 1.45 NA, 100× oil immersion objective lens (UPlanSApo, Olympus) and 1.6× tube lens giving a total magnification of 160×. A 525 nm bandpass filter (FF03-525/50-25, Semrock) was used in the detection path. Finally, images (512×512 pixels, 16 μm pixel size) were acquired under frame transfer mode at 33 fps.

In general, for relaxed rings the two strands can be discerned, especially during the relaxation phase after the cessation of planar extensional flow (Fig. S1, top); while for linear DNA molecules, the contour length is twice that of their ring counterparts making them easily distinguishable from ring DNAs (Fig. S1, bottom). Supercoiled molecules all exhibit single 'ribbon-like' structures, which are essentially linear rather than branched, after being stretched (Fig. S1, middle). By comparing the extended conformations of supercoiled and linear molecules of the same length L we can see that the supercoiled DNA 'length' appears to be comparable to the $0.4L$ value reported in Ref [5] that we use to compute R_G and thus c^* (described in following section).

Beyond revealing the structures assumed by the topologically-distinct molecules, the results of our single-molecule analysis yielded a blend composition of ~69% rings, ~26% supercoiled molecules, and 5% linear chains. While this makeup is close to that obtained via gel electrophoresis it does reveal the presence of a small fraction of linear chains. However, based on our previous steady-state diffusion studies for ring-linear DNA blends[6], we do not expect that this small fraction plays a significant role in the results we present. In the referenced study (Ref [6]) we showed that for a comparable DNA length and concentration (45 kbp, 0.5 mg/ml), the introduction of 5% linear chains into a ring DNA solution only reduced the diffusion of ring DNA by ~3%. This is compared to the 21% drop measured at ~25%. Because the supercoiled contaminants, which appear to assume conformations akin to shorter linear chains, make up >25% of the blend, we conclude that it is the presence of supercoiled constructs rather than linear chains that play the dominant role in the intriguing mechanics we report.

Further, we note that the pipetting method to introduce DNA molecules into the flow device, as well as the extra handling involved in labeling molecules, can introduce nicks in rings, thus overestimating the fraction of linear chains. In microrheology experiments, we use wide-bore pipet tips (not possible for microfluidics experiments) and only require a single pipetting step. As such, the 5% linear chains that single-molecule experiments measure is quite likely an overestimate. We nonetheless take it into account when computing the overlap concentration (see below) and interpreting our experimental results.

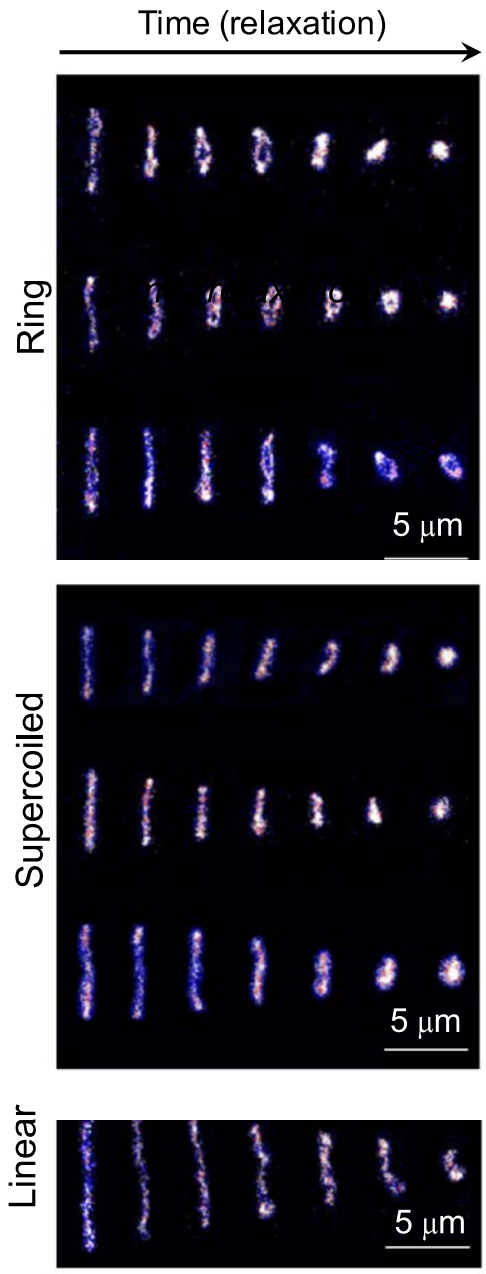

Figure S1. Single-molecule 'counting' experiments to visualize DNA molecules in the blend. Single-molecule snapshots of 50 kbp relaxed ring (top), supercoiled (middle) and linear (bottom) DNA molecules within the same sample during the relaxation phase after stretching under planer extensional flow. 231 molecules in total were stretched and imaged during relaxation to determine that ring, supercoiled and linear molecules comprise 69%, 26% and 5% of the blend.

Overlap Concentration Determination: Measurements were performed with dilutions of this sample to 0.14, 0.27, 0.41 and 0.51 mg/mL, chosen to span from ~2*x* below to ~2*x* above *c** (Fig. 1a). To determine an effective *c** for blends we start with the expression $c^*=(3/4\pi)M/N_A R_G^3$ that is conventionally used in the literature. This expression is derived by equating the solution volume (m/c^*, where m is total mass) to the total volume the molecules comprise, i.e. the total number of molecules ($N=mN_A/M$) multiplied by the volume per molecule ($V_m=4\pi R_G^3/3$). We use this approach but consider that each component contributes separately to the total volume the molecules fill in solution: $N_S V_{m,S}+N_R V_{m,R}+N_L V_{m,L} = (4\pi/3)N(0.69R_{G,R}^3+0.26R_{G,S}^3+0.05R_{G,L}^3)$. The resulting expression is then:

$$c^*=(3/4\pi)M/N_A(0.69R_{G,R}^3+0.26R_{G,S}^3+0.05R_{G,L}^3).$$

The radius of gyration for rings has been shown to be smaller than their linear counterparts with a ratio $R_{G,L}/R_{G,R}=1.58$ measured for DNA.[1] The radius of gyration for supercoiled DNA ($R_{G,S}$) has likewise been shown to be smaller than linear chains and can be calculated via the worm-like-chain expression for linear polymers assuming a contour length of $L_S=0.4L$, where L is the contour length of the polymer:

$$R_{G,S} = p\left[\frac{0.4L}{3p} - 1 + 2\left(\frac{p}{0.4L}\right)^2\left(1 - e^{-0.4L/p}\right)\right]^{0.5},$$

where p is the persistence length (~50 nm for DNA).[5] We note that the 0.4 prefactor may depend on ionic strength (the ionic strength used in Ref 4 is higher than our conditions), and may overestimate R_G for larger DNA (as noted by authors of Ref 4). However, by comparing the extended conformations of supercoiled and linear molecules of the same length L in our blends (Fig S1) we can see that the supercoiled DNA 'length' appears to be comparable to the 0.4L value reported in Ref 4 that we use to compute R_G and thus *c**.

Using these expressions and relations, along with reported values of R_G for similarly sized ring and linear DNA, we compute $R_{G,S}\cong 0.33$ μm, $R_{G,R}\cong 0.37$ μm, and $R_{G,L}\cong 0.56$ μm. From these values we calculate $c^*\cong 0.25$ mg/mL. As such, our chosen concentrations equate to ~0.5*c**, *c**, 1.5*c** and 2*c**. For reference, *c** for the equivalent system of linear DNA is ~4*x* smaller (~74 μg/ml). Throughout the manuscript we refer to all blend concentrations in terms of *c**. In good solvent conditions (as we have here) the entanglement concentration for DNA has been shown to be ~6*c**.[7, 8]

To estimate the correlation blob size ξ_B for our system we compute a weighted average of the blob sizes for each topology using the expression $\xi_B = R_G(c/c^*)^{-3/4}$.[9, 10] The effective correlation blob size is then $\xi_B \cong (0.69R_{G,R}+0.26R_{G,S}+0.05R_{G,L})(c/c^*)^{-3/4}$ which equates to values of ~0.57 μm (0.14 mg/ml), 0.35 μm (0.27 mg/ml), 0.26 μm (0.41 mg/ml), and 0.22 μm (0.51 mg/ml). The mesh size ξ is related to the correlation blob size via $\xi = 6^{1/2}\xi_B$.[9] The mesh sizes for the 4 different blends are 1.38 μm (0.14 mg/ml), 0.88 μm (0.27 mg/ml), 0.64 μm (0.41 mg/ml), and 0.55 μm (0.51 mg/ml).

Sample Preparation: For passive and active microrheology, 1 μm and 4.5 μm carboxylated polystyrene microspheres (Polysciences, Inc.) were added to solutions, respectively. Both beads were coated with Alexa-488 BSA to prevent DNA adsorption and enable fluorescence visualization. This coating confers a no-stick boundary condition between the beads and the DNA solution. To inhibit photobleaching of microspheres, glucose (45 μg/mL), glucose oxidase (43 μg/mL), catalase (7 μg/mL) and β-mercaptoethanol (5 μg/mL) were added. 0.1% Tween-20 was also added to prevent DNA adsorption to sample chamber surfaces. Using a wide-bore pipet tip to avoid shearing, the resulting solution was pipetted into a sample chamber comprised of a microscope slide and coverslip with two pieces of double-stick tape in between. The chamber was then sealed with epoxy and allowed to equilibrate for ~15 mins before measurements.

Passive Microrheology: For passive microrheology measurements (Fig. 1b-d), diffusing microspheres were visualized using an Olympus IX73 microscope with a 20x objective and high-speed CMOS camera

(Hamamatsu Orca Flash 2.8). For each concentration, 15 time-series of 512x512 (181 nm/pixel) images consisting of ~150 beads per frame were recorded for 15 seconds at 30 fps. Custom-written MATLAB code was used to extract the trajectories of diffusing beads and calculate the mean-squared displacements (MSD) in the *x* and *y* directions. All MSDs shown consist of ~2000 particles and are an average of MSDs in *x* and *y* directions, denoted as $<\Delta r^2(t)>$. Diffusion coefficients were calculated via $<\Delta r^2(t)>=2Dt$; and linear viscoelastic moduli ($G'(\omega)$, $G''(\omega)$) were determined via the generalized Stokes-Einstein relation:[11]

$$G^*(\omega) = G'(\omega) + iG''(\omega) = \frac{k_B T}{i\omega < \Delta r^2(\omega) > \pi R},$$

where k_B is Boltzmann's constant, T is the absolute temperature, $<\Delta r^2(\omega)>$ is the Fourier transform of $<\Delta r^2(t)>$, and R the radius of the beads. The Fourier transform of $<\Delta r^2(t)>$ is obtained by:[12]

$$-\omega^2 < \Delta r^2(\omega) >= (1 - e^{-i\omega t_1}) \frac{<\Delta r^2(t_1)>}{t_1} + 2De^{-i\omega t_N} + \sum_{k=2}^{N} \left(\frac{<\Delta r^2(t_k)> - <\Delta r^2(t_{k-1})>}{t_k - t_{k-1}} \right) (e^{-i\omega t_{k-1}} - e^{-i\omega t_k}),$$

where 1 and N in the equation represent the first and last point from the oversampled MSD data. Oversampling is done using the PCHIP MATLAB function. More details about the data analysis can be found in Ref [13].

While we acquire particle trajectories over the time interval [0.033 – 15 s] corresponding to [0.42 – 188 rad/s], we only use the interval [0.25 – 15 s] in our analysis as for shorter times the frame-to-frame bead displacements are not significantly larger than the precision in centroid localization (~200 nm vs 45 nm).[14] At 0.25 s, the displacements are an order of magnitude larger than the tracking precision of ~45 nm.

Error bars shown in Fig 2e-g are determined by carrying out the particle-tracking and microrheology analysis described above on 5 sub-ensembles of the data for each concentration and determining the quantities shown for each sub-ensemble. Error bars are the standard deviation of these 5 quantities.

Active nonlinear microrheology: We use optical tweezers to apply fast mesoscale strains to the blends (Fig. 1e,f). The optical trap consists of an Olympus IX70 microscope with a 60*x* 1.4 NA objective (Olympus) and a 1064 nm Nd:YAG fiber laser (Manlight). A position sensing detector (Pacific Silicon Sensors) is used to measure the deflection of the laser beam, which is proportional to the force exerted on the trapped bead. The proportionality constant (i.e. trap stiffness) is obtained via Stokes drag method as previously described.[15, 16] Strains are applied to blends by moving a nanopositioning piezoelectric microscope stage (Mad City Labs) a fixed distance of 30 μm (Fig. 1e) at speeds of v = 5 – 200 μm/s, which are converted to strain rates via $\dot{\gamma}=3v/\sqrt{2}R$.[17] Both stage position and laser deflection data are acquired at 20 kHz before (5 s, equilibrium), during (0.15-6 s, strain) and following (9-15 s, relaxation) the strain (Fig. 1f).

The nanopositioning stage takes 0.002 s to accelerate to constant speed from rest and decelerate to rest following constant rate strain (Fig. S2). As such, the force data we show during the strain phase is only for the portion of the strain that is at constant speed (chopping off the initial and final 0.002 s of data). Likewise, the relaxation data shown starts 0.002 s after the stage begins to stop (once it has come to complete halt).

At least 15 trials, each with a new bead in a new unperturbed location, are conducted for every speed and concentration in order to verify homogeneity throughout the sample and reproducibility of the force values. All displayed data is the average and standard error of all trials for each condition.

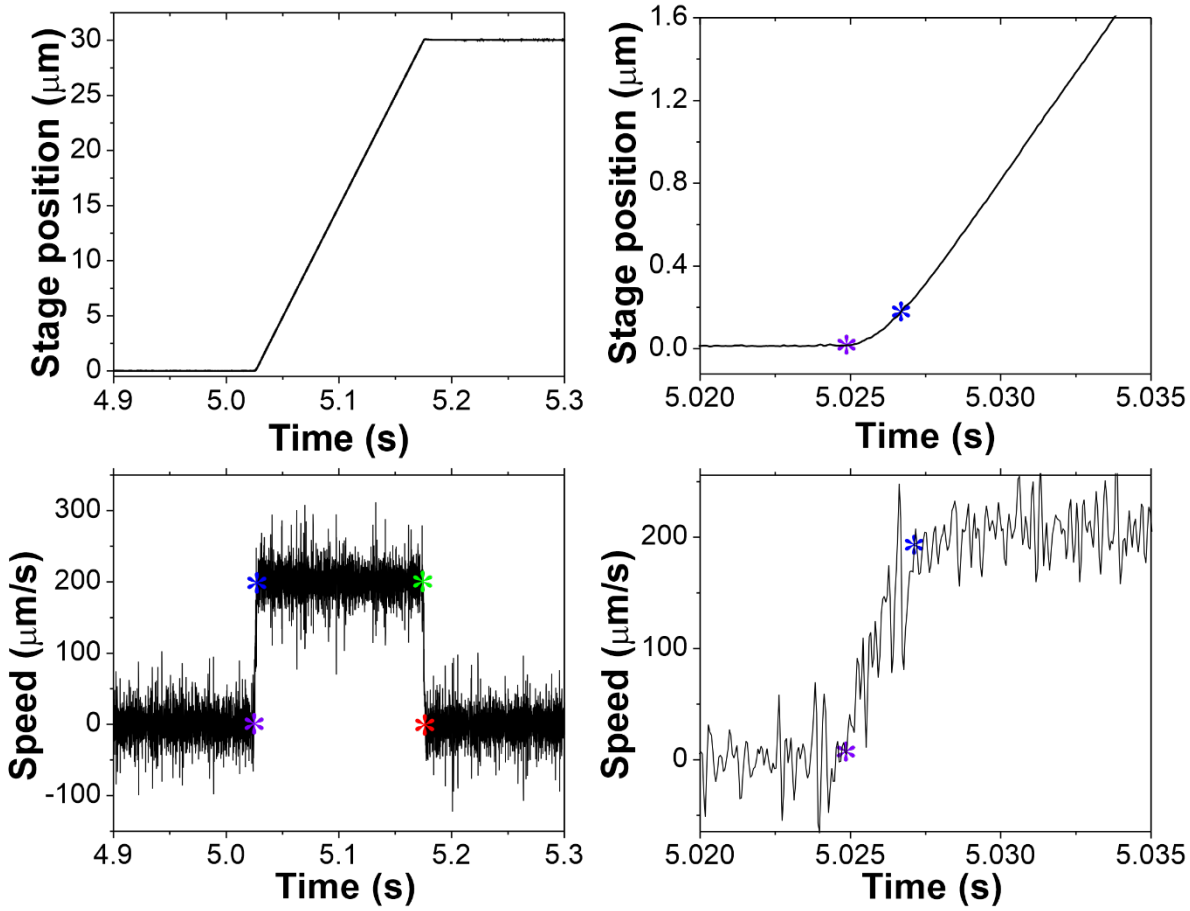

Figure S2. Position and velocity of nanopositioning stage during active microrheology measurement. (Top left) Stage position during all phases of a 200 μm/s strain experiment. (Top right) Zoom-in of the start of the stage motion. A constant slope (i.e. 200 μm/s) is achieved in ≤0.002 s (indicated by violet and blue stars). (Bottom left) Stage velocity during all phases of a 200 μm/s strain experiment. For the strain phase, we evaluate force curves during the time at which stage maintains constant speed (indicated by blue and green stars. For the relaxation phase, we evaluate force curves once the stage comes to a complete stop (indicated by red star). (Bottom right) Zoom-in of the start of the strain phase. As shown, the stage takes ≤0.002 s to reach constant speed from rest. Stage takes identical time to come to rest following constant speed strain.

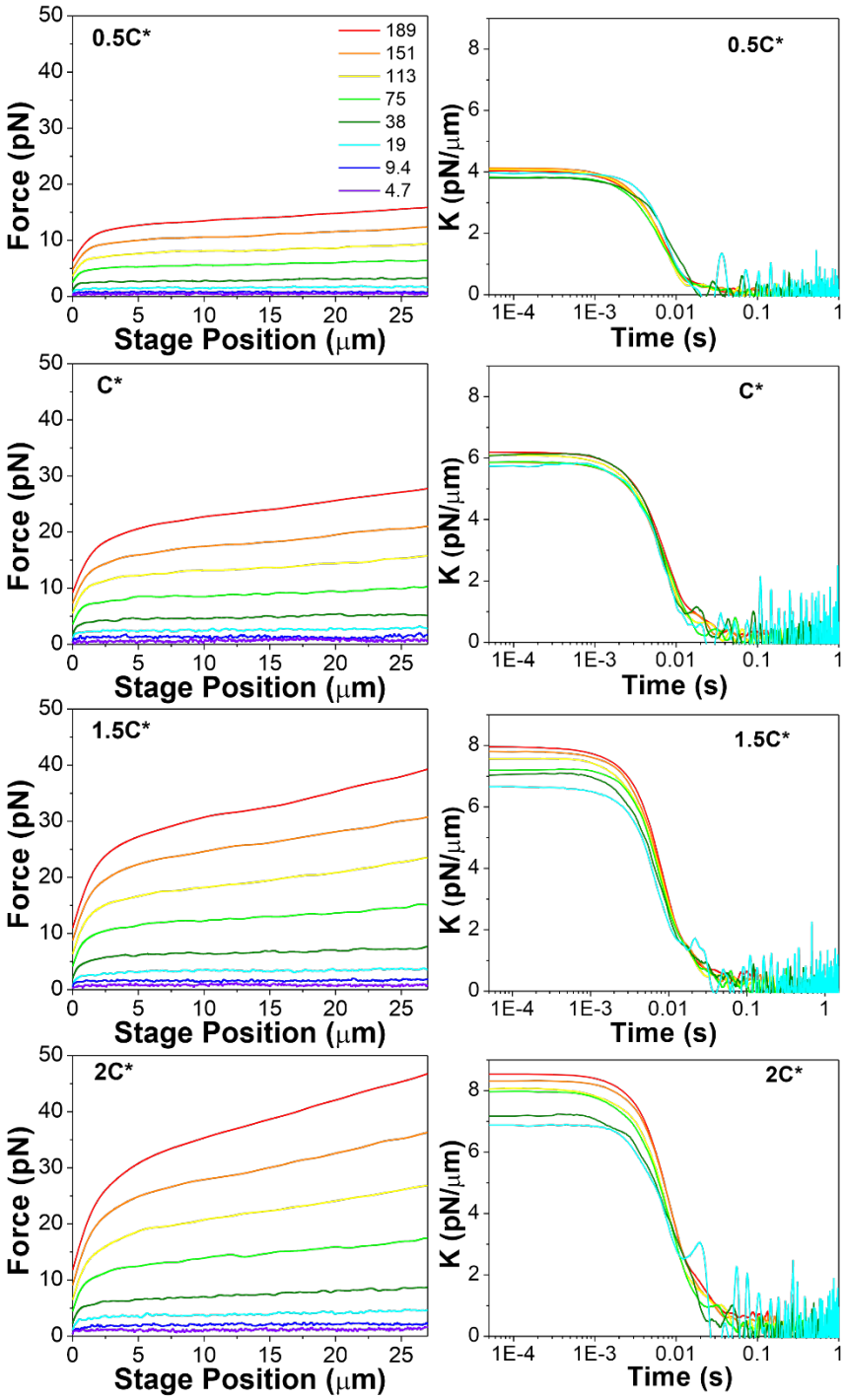

Figure S3. Nonlinear force response of blends of ring and supercoiled DNA. Measured force (left) and corresponding differential modulus, $K=dF/dx$, (right) in response to 30 μm strains with $\dot{\gamma}$ listed in units of s^{-1} in legend (top left). The blend concentration is listed in units of c^* at the top of each plot. For a given concentration, force increases with increasing $\dot{\gamma}$. Similarly, for a given $\dot{\gamma}$, force increases with increasing c. For $c<c^*$, dependence of K on $\dot{\gamma}$ is negligible but becomes significant for $c>c^*$. At any given $\dot{\gamma}$, initial K value increases with increasing concentration.

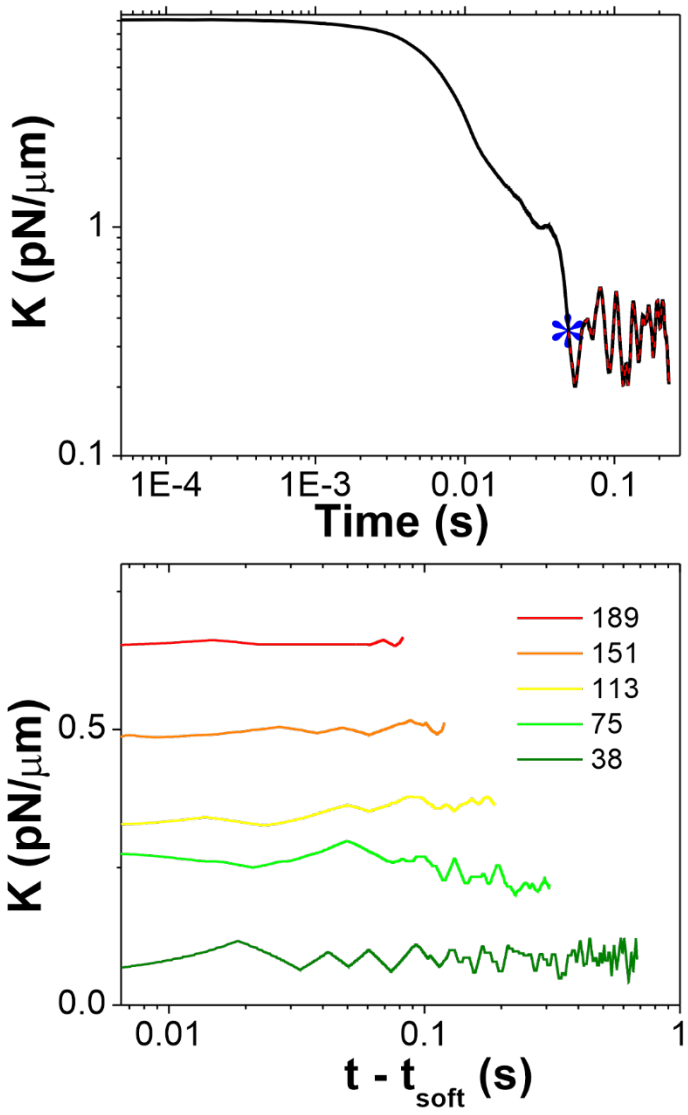

Figure S4. Final phase of differential modulus in response to nonlinear strains. (Top) A sample K vs t curve ($2c^*$, $\dot{\gamma}$=113 s^{-1}). Blue star indicates the time we define as t_{soft} and red dashes indicate the region averaged over to compute K_f. (Bottom) The final plateau regions of K vs t curves for $2c^*$, smoothed using a 2500-5000 point moving median (MATLAB). $\dot{\gamma}$ are listed in units of s^{-1} in legend.

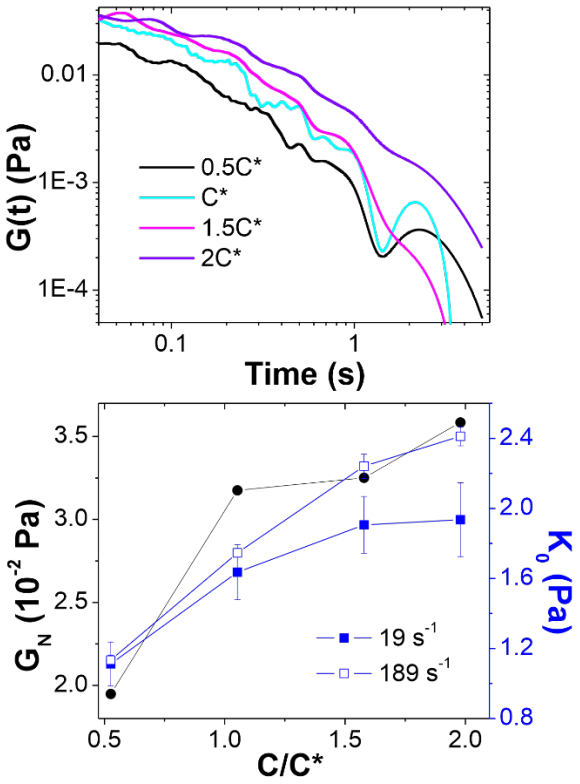

Figure S5. Linear relaxation modulus *G(t)* and initial values of *G(t)* and the nonlinear differential modulus *K*. (Top) Linear relaxation modulus *G(t)* computed from the viscoelastic moduli *G'* and *G''* using the numerical formula provided in Ref [18]. (Bottom) The initial *G(t)* value G_N (left axis) and the initial nonlinear differential modulus value K_0 versus blend concentration in units of *c**.

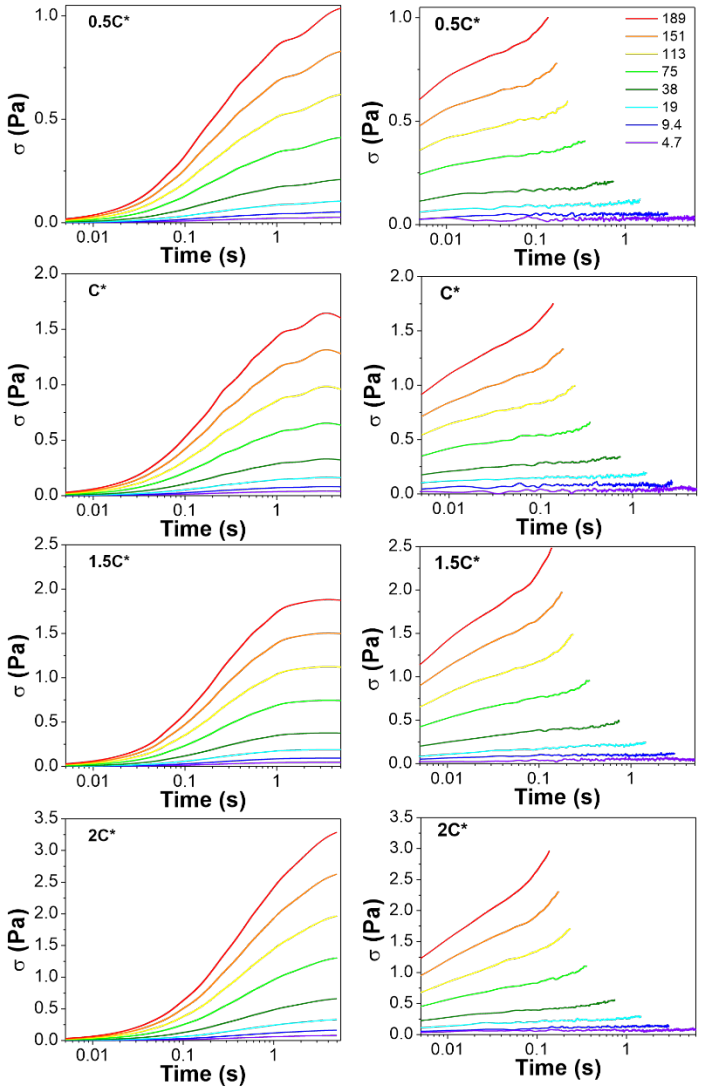

Figure S6. Expected LVE stress growth compared to the nonlinear stress growth measured in nonlinear microrheology experiments. (Left column) LVE stress growth is computed via $\sigma(t) = \dot{\gamma} \int_0^t G(t)\, dt$.[19] (Right column) Nonlinear force (F) growth data from Fig. S3 is converted into stress via $\sigma = F/\pi R^2$ where R is the bead radius.[17] There is a clear distinction between LVE stress growth and nonlinear stress growth. In LVE regime, stress reaches a steady state given sufficient time at all strain rates but strain stiffening is increasingly observed with increasing strain rate in nonlinear regime.

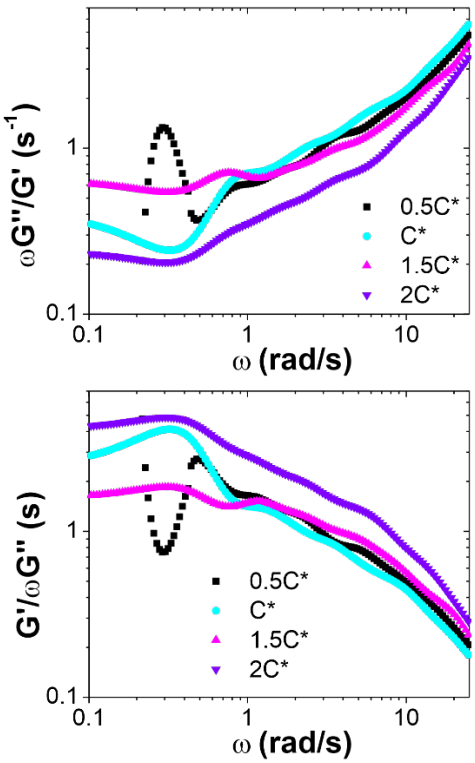

Figure S7. Terminal linear regime relaxation frequency and time determined from passive microrheology experiments. (Top) Terminal relaxation frequencies, $\omega_T = \lim_{\omega \to 0} \omega G''/G'$, are well below experimental nonlinear strain rates ($\dot{\gamma}$=4.7-189s^{-1}) for all blends, a criterion for nonlinearity. Applied nonlinear strain ($\gamma=\dot{\gamma}t$=6.7) also far exceeds the critical value of ~1 for the onset of nonlinearity. γ is calculated by dividing stage displacement by the diameter of beads (*2R*).[17] (Bottom) Terminal relaxation times, $= \lim_{\omega \to 0} G'/\omega G''$, in the linear regime are an order of magnitude slower than the slowest relaxation time measured in the nonlinear regime (i.e. $\tau_3 \cong 0.15$ s). This mismatch indicates that in the linear regime the blend dynamics are similar to those of entangled linear polymers while in the nonlinear regime the blends respond similarly to entangled rings.

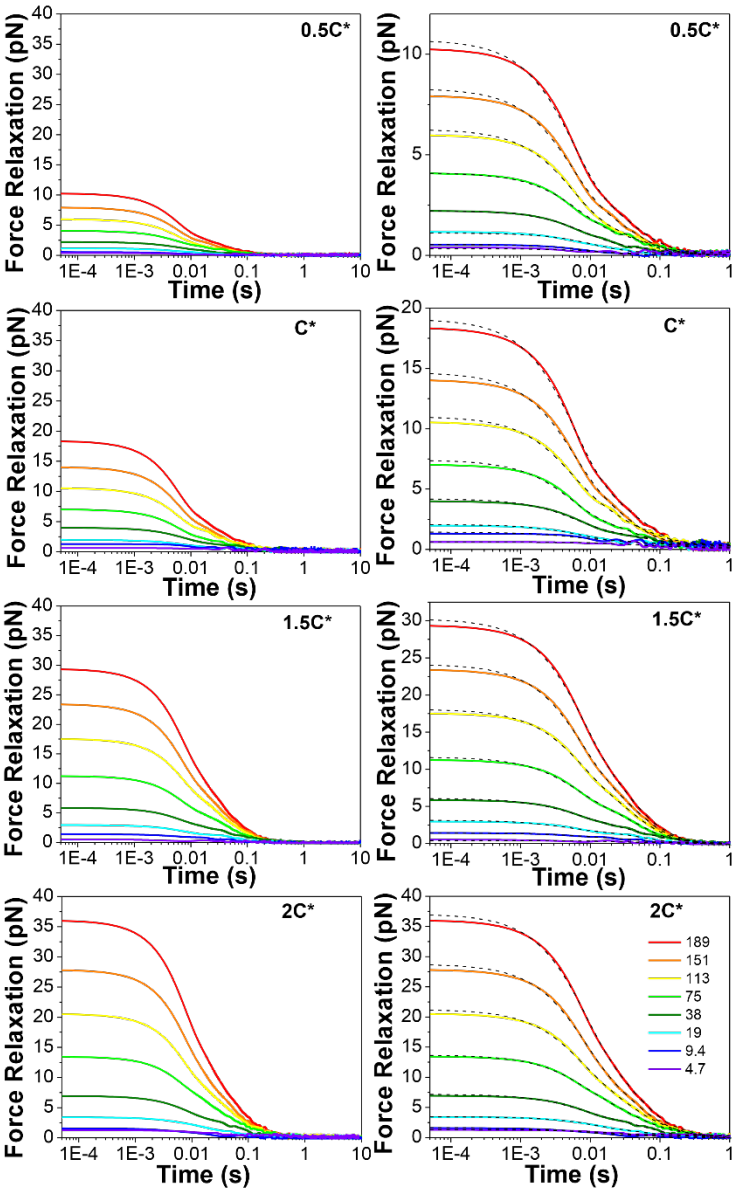

Figure S8. Relaxation of force induced in ring-supercoiled DNA blends following nonlinear strains. (Left) Measured force relaxations following 30 μm strains with $\dot{\gamma}$ listed in units of s^{-1} in legend (top plot). (Right) Zoom-ins of relaxations with corresponding fits to exponential decay functions (black dashed lines). The blend concentration is listed in units of c^* at the top of each plot. For $\dot{\gamma}$>40 s^{-1}, relaxations are well-fit to a sum of three exponential decays (i.e. $F(t)=C_1e^{-t/\tau1}+C_2e^{-t/\tau2}+C_3e^{-t/\tau3}$). For lower strain rates, single and double mode exponential decay functions are sufficient to fit the data (see Fig S9).

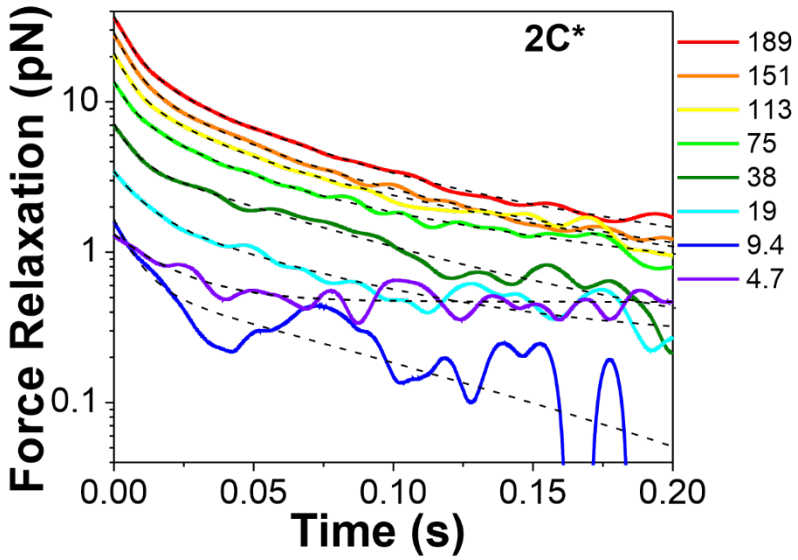

Figure S9. Initial force relaxation following nonlinear strain. Bottom-right plot of Fig S8 replotted on linear-*x* log-*y* scale and truncated to 0.20 s. Dashed lines are corresponding fits to exponential decay functions. $\dot{\gamma}$ listed in units of s^{-1} in legend (top plot). Note that force decay begins immediately and is initially fast (τ_1 and τ_2 relaxation) then slows to a steady exponential decay (constant slope, τ_3).

REFERENCES

1. R. M. Robertson, S. Laib and D. E. Smith, *Proceedings of the National Academy of Sciences*, 2006, **103**, 7310-7314.
2. S. Laib, R. M. Robertson and D. E. Smith, *Macromolecules*, 2006, **39**, 4115-4119.
3. J. F. Marko and E. D. Siggia, *Physical Review E*, 1995, **52**, 2912-2938.
4. Y. Zhou and C. M. Schroeder, *Physical Review Letters*, 2018, **120**, 267801.
5. D. R. Latulippe and A. L. Zydney, *Biotechnol Bioeng*, 2010, **107**, 134-142.
6. C. D. Chapman, S. Shanbhag, D. E. Smith and R. M. Robertson-Anderson, *Soft Matter*, 2012, **8**, 9177-9182.
7. R. M. Robertson and D. E. Smith, *Macromolecules*, 2007, **40**, 3373-3377.
8. S. Pan, D. A. Nguyen, T. Sridhar, P. Sunthar and J. R. Prakash, *Journal of Rheology*, 2014, **58**, 339-368.
9. M. Tanoguchi and Y. Murayama, *AIP Advances*, 2018, **8**, 105218.
10. J. R. Prakash, *Current Opinion in Colloid & Interface Science*, 2019, **43**, 63-79.
11. T. G. Mason and D. A. Weitz, *Physical Review Letters*, 1995, **74**, 1250-1253.
12. R. M. L. Evans, M. Tassieri, D. Auhl and T. A. Waigh, *Physical Review E*, 2009, **80**, 012501.
13. M. Tassieri, R. M. L. Evans, R. L. Warren, N. J. Bailey and J. M. Cooper, *New Journal of Physics*, 2012, **14**, 115032.
14. T. Savin and P. S. Doyle, *Biophysical Journal*, 2005, **88**, 623-638.
15. C. D. Chapman and R. M. Robertson-Anderson, *Physical Review Letters*, 2014, **113**, 098303.
16. W. J. Weigand, A. Messmore, J. Tu, A. Morales-Sanz, D. L. Blair, D. D. Deheyn, J. S. Urbach and R. M. Robertson-Anderson, *PLOS ONE*, 2017, **12**, e0176732.
17. T. M. Squires, *Langmuir*, 2008, **24**, 1147-1159.
18. F. R. Schwarzl, *Rheologica Acta*, 1975, **14**, 581-590.
19. R. A. Pethrick, *Polymer International*, 2004, **53**, 1394-1395.